

UC Berkeley

UC Berkeley Previously Published Works

Title

Mechanism and Kinetics of n-Butane Dehydrogenation to 1,3-Butadiene Catalyzed by Isolated Pt Sites Grafted onto \square SiOZn-OH Nests in Dealuminated Zeolite Beta

Permalink

<https://escholarship.org/uc/item/0ch4g7f4>

Journal

ACS Catalysis, 12(6)

ISSN

2155-5435

Authors

Zhang, Yanfei
Qi, Liang
Leonhardt, Branden
[et al.](#)

Publication Date

2022-03-18

DOI

10.1021/acscatal.2c00059

Peer reviewed

Mechanism and Kinetics of *n*-Butane Dehydrogenation to 1,3-Butadiene Catalyzed by Isolated Pt Sites Grafted onto ≡SiOZn–OH Nests in Dealuminated Zeolite Beta

Yanfei Zhang,[§] Liang Qi,[§] Branden Leonhardt, and Alexis T. Bell*



Cite This: *ACS Catal.* 2022, 12, 3333–3345



Read Online

ACCESS |



Metrics & More



Article Recommendations



Supporting Information

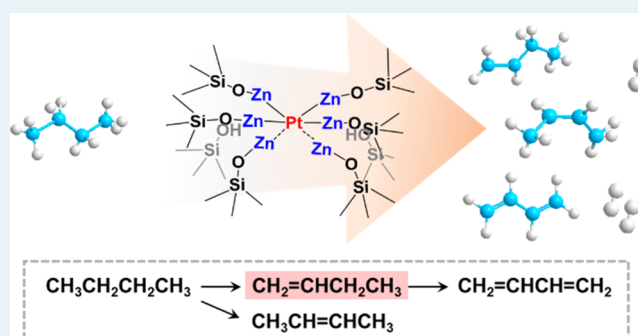
ABSTRACT: An interest in the on-purpose production of 1,3-butadiene (1,3-BD) has grown, as a consequence of the decline in naphtha cracking for the production of ethene and propene, products that can now be produced economically by thermal dehydrogenation of ethane and propane contained in natural gas. In this study, the mechanism and kinetics of *n*-butane dehydrogenation to 1,3-BD are explored over atomically distributed Pt sites grafted onto dealuminated zeolite BEA (DeAlBEA) in the form of (≡Si–O–Zn)_{4–6}Pt complexes. Reaction of *n*-butane dehydrogenation carried out at 823 K with 2.53 kPa *n*-butane/He and a weight-hourly space velocity (WHSV) of 14.5 h^{−1} produced 1,3-BD with a turnover frequency of 0.45 mol 1,3-BD (mol Pt)^{−1} s^{−1}.

Space-time studies and identification of the reaction intermediates suggest that *n*-butane first undergoes dehydrogenation primarily to 1-butene, which then rapidly isomerizes to produce an equilibrated mixture of 1-butene and 2-butene. 1-Butene then undergoes secondary dehydrogenation to produce 1,3-BD. We report, here, a detailed study of the kinetics of *n*-butane dehydrogenation to butenes and 1-butene dehydrogenation to 1,3-BD over isolated Pt sites. Both reactions exhibit a Langmuir–Hinshelwood dependence on *n*-butane and 1-butene partial pressures, respectively. Comparison of effective forward rate constants of *n*-butane dehydrogenation to butenes (*k*_{1f}) and butene dehydrogenation to 1,3-BD (*k*_{2f}) shows that the isolated Pt sites grafted onto DeAlBEA exhibit a very high activity for sequential dehydrogenation of *n*-butane to 1,3-BD relative to other Pt-based catalysts previously reported.

KEYWORDS: *n*-butane dehydrogenation, 1,3-butadiene, kinetics, isolated Pt sites, dealuminated Beta zeolite

1. INTRODUCTION

1,3-Butadiene (1,3-BD) is widely used as a monomer in the manufacture of synthetic rubbers and a range of polymers.¹ The global demand for 1,3-BD is estimated to reach 19.6 million tons by 2027 and to increase thereafter at a rate of 4.5% per annum driven by the increasing demand for synthetic rubber in the automobile, health care, building, and construction sectors.² Conventionally, 95% of the global production of 1,3-BD is obtained by cryogenic extractive distillation of the C₄ fraction derived from naphtha steam cracking, which is used primarily to produce ethene and propene.^{3,4} With the increasing availability of inexpensive shale gas, the production of ethene and propene has gradually shifted to direct dehydrogenation of ethane and propane present in the liquid fraction of shale gas. This change has diminished the extent to which naphtha cracking is carried out and has had serious consequences for the production of 1,3-BD.^{1,5,6} Consequently, there is growing interest in using *n*-butane from liquified petroleum gas and naphtha for on-purpose *n*-butane dehydrogenation (BDH) to 1,3-BD.^{7–9}

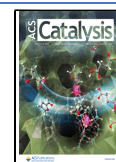


Dehydrogenation of *n*-butane and/or *n*-butene to 1,3-BD can be divided into nonoxidative thermal dehydrogenation and oxidative dehydrogenation routes. While the latter process mitigates the thermodynamic equilibrium limitation of thermal dehydrogenation, it is generally characterized by low alkene selectivity due to overoxidation of alkenes to CO₂.¹⁰ By contrast, the direct dehydrogenation of *n*-butane produces 1,3-BD, butenes together with H₂, all of which are valuable products.¹ Despite achievements in technologies for direct dehydrogenation of *n*-butene or *n*-butane/*n*-butene mixtures (e.g., Houdry–Catadiene process), *n*-butene is generally used as the feedstock to achieve a high yield of 1,3-BD. Compared with significant improvements in product selectivity achieved

Received: January 4, 2022

Revised: February 1, 2022

Published: February 28, 2022



for ethane and propane dehydrogenation, catalysts for direct *n*-butane dehydrogenation to 1,3-BD with high selectivity have proven more difficult to identify,^{1,11} and in studies reported to date, the 1,3-BD selectivity is generally less than 20%.^{8,12,13}

Supported Pt catalysts and Pt bimetallic catalysts, particularly PtSn, have been widely explored for direct dehydrogenation of alkanes to alkenes. Catalysts containing very small Pt, PtSn, or PtZn nanoclusters have been shown to be highly active, selective, and resistant to coking.^{14,15} Pt nanoclusters dispersed on supports such as SiO₂, SBA-15, Al₂O₃, and graphene have also been investigated for *n*-butane dehydrogenation.^{7,8,16,17} Here too, it has been found that small Pt ensembles are desirable since they minimize the activity for structure-sensitive side reactions, such as C–C cracking, skeletal isomerization, and deep dehydrogenation to coke.^{16,17} It is, therefore, reasonable to expect that small nanoclusters or even single atoms of Pt might be highly active and selective for the production of 1,3-BD via *n*-butane dehydrogenation.^{17–19} This line of reasoning is further stimulated by recent studies of propane dehydrogenation, which have shown that the incorporation of a second metal, such as Cu, Zn, Fe, and Sn, helps to segregate Pt atoms and tailor their electronic state.^{19–23} The results of published studies indicate that highly dispersed, electron-rich Pt atoms exhibit high alkene selectivity and low activity for carbon deposition. Despite the progress made in developing Pt bimetallic catalysts, most of these catalysts contain clusters or nanoparticles, which still exhibit a moderate tendency to form coke and, for larger particles, low Pt atom utilization.

We have recently shown that isolated Pt atoms can be stabilized by interaction with ≡SiOZn–OH nests formed in the silanol nests of dealuminated zeolite BEA (DeAlBEA).²⁴ Pt grafted onto the ≡SiOZn–OH nests produces (≡Si–O–Zn–O)_{4–6}Pt complexes, which are easily reduced to (≡Si–O–Zn)_{4–6}Pt complexes. The isolated (≡Si–O–Zn)_{4–6}Pt sites exhibit very high activity, selectivity, and stability for propane dehydrogenation. Encouraged by these results, we have investigated the performance of these sites for *n*-butane dehydrogenation to 1,3-BD. For typical reaction conditions, 2.53 kPa *n*-butane/He, 823 K, and weight-hourly space velocity (WHSV) = 14.5 h^{–1}, 0.04Pt–0.36Zn–DeAlBEA (with molar ratios of Zn and Pt to Al in parent H-BEA zeolite of 0.36 and 0.04, respectively) exhibits an *n*-butane conversion of 66% and a 1,3-BD selectivity up to 35.3%. The isolated Pt sites in 0.04Pt–0.36Zn–DeAlBEA exhibit an effective forward rate coefficient for *n*-butane dehydrogenation to butene (*k*_{1f}) that is among the best and the highest butene dehydrogenation to 1,3-BD (*k*_{2f}) relative to other reported Pt-based catalysts. Space-time studies combined with the identification of the primary reaction intermediates show that 1-butene is the kinetically favored source of 1,3-BD.

2. EXPERIMENTAL SECTION

2.1. Catalyst Preparation. **2.1.1. Preparation of Zn-DeAlBEA.** Commercial H-BEA (BASF Co.) with a Si/Al ratio of 13 determined by ICP-OES, (Galbraith Laboratories, Inc.) was calcined to remove organic species by heating the zeolite in a muffle furnace at 2 K min^{–1} from ambient temperature to 823 K in static air and then holding at this temperature for 4 h. H-Beta thus formed was then dealuminated to siliceous Beta (dealuminated Beta zeolite, DeAlBEA) by suspending it in 13 M nitric acid solution held at 373 K for 20 h with rigorous stirring. The resulting white powder was filtered, washed

thoroughly with deionized water until the pH of the supernatant was 6–7, then dried at 373 K under vacuum overnight, and stored in vacuum.²⁷ Al NMR revealed that all of the aluminum contained in the parent zeolite was removed by the dealumination process described above.²⁴

Zn-DeAlBEA was prepared by incipient wetness impregnating DeAlBEA with an aqueous solution of Zn(NO₃)₂ (Alfa Aesar, 99%) and subsequent drying at room temperature for 5 h, at 323 K for 2 h, and finally at 823 K for 6 h in static air. The weight loading of Zn in Zn-DeAlBEA studied here used for the present studies was 2.4 wt %. Further details of the preparation protocol are given in ref 24. The resulting sample is designated as 0.36Zn–DeAlBEA, where 0.36 stands for the molar ratio of Zn/Al (the molar amount of Al is in the H-BEA parent).

2.1.2. Preparation of Pt-Zn-DeAlBEA and Pt-DeAlBEA. Pt-Zn-DeAlBEA and Pt-DeAlBEA with Pt weight loadings of around 0.8 wt % were prepared via wetness impregnation utilizing (NH₃)₄Pt(NO₃)₂ as the Pt precursor and Zn-DeAlBEA and DeAlBEA as supports, respectively. Typically, 0.7 mL of the aqueous solution of (NH₃)₄Pt(NO₃)₂ was used for 0.25 g of support. The Pt-impregnated material was dried at room temperature and then at 353 K before being calcined at 623 K for 2 h in static air. The final products are designated as 0.04Pt–0.36Zn–DeAlBEA and 0.04Pt–DeAlBEA, respectively, where 0.04 designates the Pt/Al molar ratio. To explore the effect of Pt contents, catalysts with different Pt contents were prepared by changing the concentrations of Pt precursor in impregnating solutions. These materials are designated as *x*0.04Pt–0.36Zn–DeAlBEA (*x* = 0.06 and 0.08, indicating the Pt/Al molar ratios of 0.06 and 0.08, respectively). The molar amount of Al is taken as that in the parent H-BEA zeolite. A detailed description of the physical characteristics of *x*0.04Pt–0.36Zn–DeAlBEA is given in ref 24. As described in this study, Pt atoms are ultimately stabilized primarily as (≡Si–O–Zn)_{4–6}Pt complexes, which are found to be highly active centers for propane dehydrogenation. By contrast, Pt dispersed on DeAlBEA (0.04Pt–DeAlBEA) is present as 5–10 nm nanoparticles, which shows much lower propane dehydrogenation activity, selectivity, and stability.

2.2. Catalyst Evaluation. The reaction of *n*-butane was conducted at atmospheric pressure using a tubular, quartz, plug-flow reactor (6.35 mm OD with an expanded section of ~12.7 mm OD). Quartz wool was placed below the catalyst bed to hold the catalyst in place, and a K-type thermocouple (Omega) was fixed at the center of the catalyst bed to detect and maintain the catalyst temperature. Generally, 10 or 20 mg of catalyst was diluted with 40 mg of silica (Silicycle, 120–200 μm). The flow rates of gaseous reactants were controlled using mass flow controllers. Concentrations of reactants and products were analyzed using an Agilent 6890A gas chromatography (GC) equipped with a GC-Alumina capillary column (50 m × 0.53 mm) and a flame ionization detector.

Prior to reaction, the catalyst was pretreated with either He (Praxair, 99.999%, 30 mL min^{–1}) for Zn-DeAlBEA or 9.04% H₂ diluted in He (Praxair, 22.2 mL min^{–1}) for Pt-DeAlBEA at 823 K for 40 min and then cooled to the reaction temperature. Specifically, after pretreatment under H₂/He, the reactor was further purged with flowing He (Praxair, 99.999%, 30 mL min^{–1}) for about 20 min before initiating the reaction.

To determine catalyst performance, *n*-butane (Matheson, 99.999%) diluted in He (Praxair, 99.999%) to an *n*-butane partial pressure of 2.53 kPa was fed to the reactor. The total rate of *n*-butane dehydrogenation was determined from the

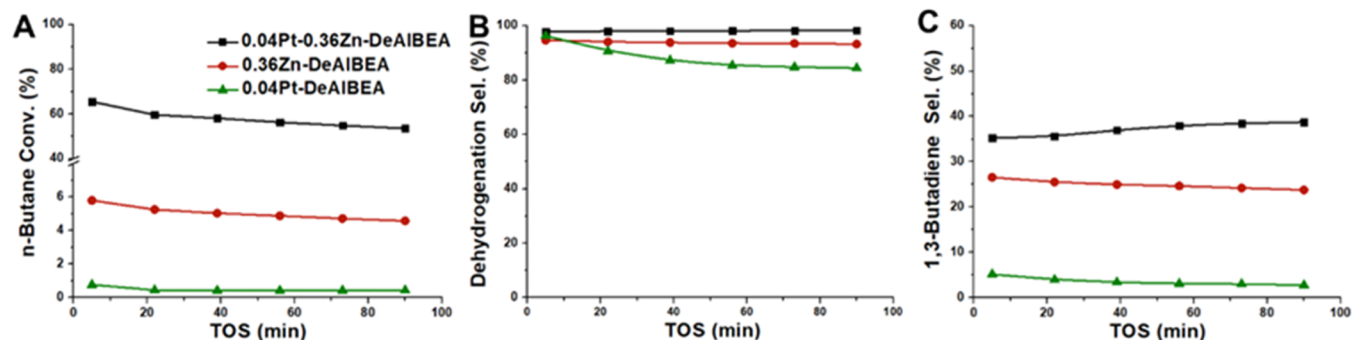


Figure 1. (A) Conversion of *n*-butane, (B) the selectivity to dehydrogenation products (butenes and 1,3-BD), and (C) the selectivity to 1,3-BD as functions of time on stream (TOS) for 0.36Zn-DeAlBEA, 0.04Pt-DeAlBEA, and 0.04Pt–0.36Zn-DeAlBEA, measured at 823 K with 2.53 kPa *n*-butane/He and WHSV = 14.5 h^{−1}. Black lines are for 0.04Pt–0.36Zn-DeAlBEA, dark red lines are for 0.36Zn-DeAlBEA, and green lines are for 0.04Pt-DeAlBEA.

sum of butene isomers (1-butene, *trans*-2-butene, *cis*-2-butene, and isobutene) and 1,3-BD. The dehydrogenation selectivity toward C₄ alkenes and diene for 0.04Pt–0.36Zn-DeAlBEA was very high (>97.9% on carbon basis at 823 K), and only trace amounts of products derived from *n*-butane cracking were observed.

The effects of space-time (defined as 1/WHSV, g catalyst-min/g *n*-butane or g catalyst-min/g 1-butene) for the reaction of *n*-butane and 1-butene, respectively, were investigated for temperatures between 553 and 623 K and total flow rates between 60 and 400 mL min^{−1}. For studies of the kinetics of *n*-butane dehydrogenation, the reaction temperature was lowered to 573–623 K and the total flow rate was set at 240 mL min^{−1} to reduce the *n*-butane conversion to <8% for the lowest partial pressure and the highest temperature studied. Studies of the kinetics of 1-butene dehydrogenation to 1,3-BD were conducted at temperatures of 583–613 K and a total gas flow rate at 120 mL min^{−1}.

2.3. Calculation for Equilibrium Distribution of *n*-Butane and 1-Butene Conversion. Equilibrium distributions of both *n*-butane and 1-butene conversions for specified reactant partial pressures and reaction temperatures and equilibrium constants were calculated utilizing Aspen Plus V12. Due to the high selectivity toward dehydrogenation products, C–C cracking was not considered. Standard Gibbs free energies of formation and standard enthalpies of formation were taken from the PURE37 database developed by the AIChE DIPPR data compilation project.²⁵ Values from this database were in excellent agreement with values taken from the NIST webbook (Table S1).²⁶ The Peng–Robinson equation of state was chosen to compute contributions from nonidealities. The Gibbs reactor module (RGibbs) was used to compute the equilibrium mole fractions, which minimizes the Gibbs free energy of the mixture under the constraints of mass balance (atom balance).

3. RESULTS AND DISCUSSION

3.1. *n*-Butane Conversion over Zn-DeAlBEA, Pt-DeAlBEA, and Pt-Zn-DeAlBEA. *n*-Butane dehydrogenation was carried out over 0.36Zn-DeAlBEA, 0.04Pt-DeAlBEA, and 0.04Pt–0.36Zn-DeAlBEA under identical reaction conditions. Figure 1 shows the variation of *n*-butane conversion and overall selectivity to dehydrogenation products (butenes and 1,3-BD) and the selectivity to 1,3-BD with time on stream (TOS) for 0.04Pt-DeAlBEA, 0.36Zn-DeAlBEA, and 0.04Pt–0.36Zn-DeAlBEA at 823 K. The overall product distributions

calculated on a carbon basis at the initial stage of *n*-butane conversion (TOS = 5 min) are presented in Figure S1 for all three catalysts. As shown in Figure 1, 0.04Pt-DeAlBEA exhibits an *n*-butane conversion of <1% and a selectivity to 1,3-BD of only 5.2%. The selectivity to C₁–C₃ cracking products is about 3.8% and increases up to 15.5% for TOS = 90 min. This result is consistent with the fact that 0.04Pt-DeAlBEA contains Pt nanoparticles²⁴ and previous findings that Pt nanoparticles favor structure-sensitive cracking reactions compared with Pt single sites and very small clusters.^{8,19} For 0.36Zn-DeAlBEA, the initial conversion of *n*-butane is 5.8% and the selectivity to 1,3-BD is 26.6%. This catalyst exhibits mild deactivation with TOS, during which the selectivity of 1,3-BD also decreases.

For 0.04Pt–0.36Zn-DeAlBEA, the initial *n*-butane conversion is 66.0% and the selectivity to 1,3-BD is 35.3 and 61.0% to linear butenes (1-butene, *trans*-, and *cis*-2-butene) and only 1.6% to isobutene, and the selectivity to C₁–C₃ products produced by both central and terminal cracking of *n*-butane accounts for about 2.1%. Since the conversion of *n*-butane is high, it is pertinent to ask how the observed *n*-butane conversion and product distribution are compared to those expected at equilibrium. The calculations presented in Figure S2 indicate that at 823 K and an *n*-butane feed partial pressure of 2.53 kPa, the equilibrium conversion of *n*-butane is 94.1%. The equilibrium distribution of products shown in Figure S2A excludes the formation of isobutene since for the conditions shown in Figure 1 and for all other conditions used in this study, the selectivity to this product did not exceed 1.6%. Our calculations show that for the experimental conditions chosen, the equilibrium selectivity to all butene isomers should be 61.1% and the ratio of 2-butene isomers to 1-butene should be 2.17, whereas the selectivity to 1,3-BD should be 39.0%. Therefore, for the conditions used in Figure 1, the selectivity of butenes is nearly equal to that at equilibrium, the ratio of 2-butenes to 1-butene (2.19) is close to that at equilibrium, and the selectivity to 1,3-BD is 90.6% of that at equilibrium.

To offset the deactivation of *n*-butane conversion at 823 K due to coking, H₂ was cofed with *n*-butane, an approach suggested by previous studies.^{8,14} Figure S3 shows the performance for *n*-butane dehydrogenation over 0.04Pt–0.36Zn-DeAlBEA with a 1:1 H₂/*n*-butane feed and without H₂ cofeeding at 823 K. As shown, the *n*-butane conversion decreases slowly from about 69.0 to 48.0% as the TOS is extended from 5 to 860 min in the presence of cofed H₂, which corresponds to about 46% of the conversion loss when the reaction was conducted in the absence of cofed H₂ (*n*-butane

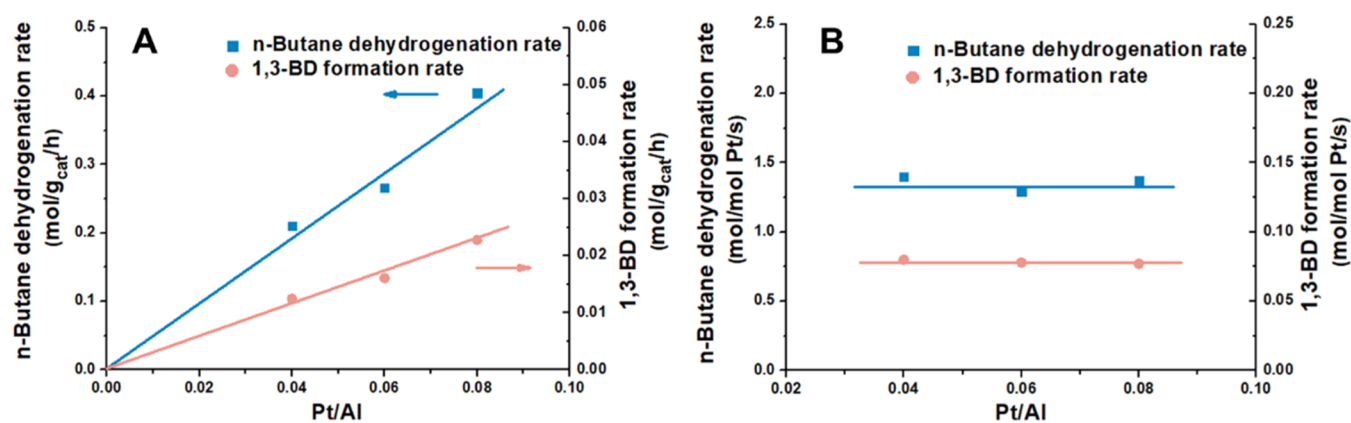


Figure 2. *n*-Butane dehydrogenation and 1,3-BD formation rates over 0.04Pt–0.36Zn–DeAlBEA measured at 2.53 kPa *n*-butane/He and 673 K as a function of Pt/Al ratio. (A) Rates normalized per gram of catalyst. (B) Rates normalized per Pt atom. Solid lines are guides for the eye. Reactions are conducted based on the same space-time relative to the Pt atom.

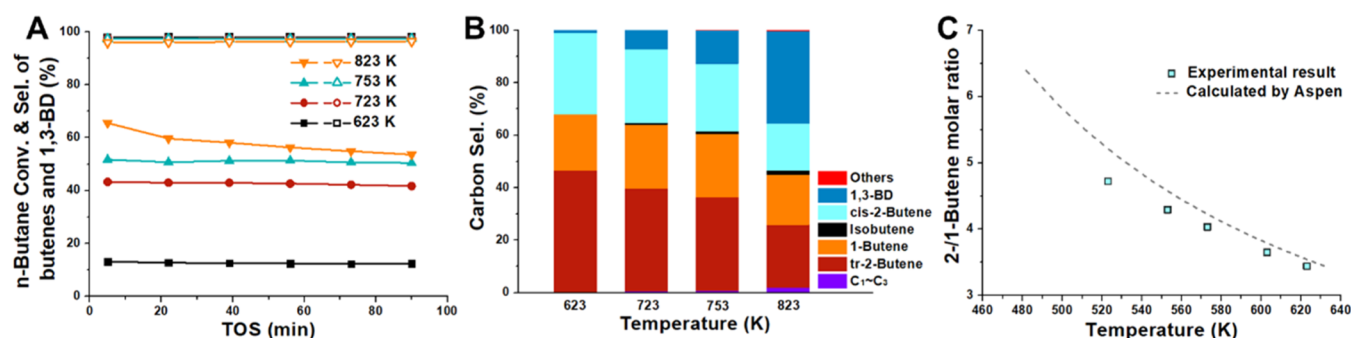


Figure 3. Effects of reaction temperature on (A) the conversion of *n*-butane and overall selectivity to butenes and 1,3-BD as functions of TOS and (B) product distributions for 0.04Pt–0.36Zn–DeAlBEA, measured with 2.53 kPa *n*-butane/He and WHSV = 14.5 h⁻¹. In panel (A), solid data points show the conversion of *n*-butane at different temperatures and the open data points show the overall selectivities to butenes and 1,3-BD. (C) Effects of reaction temperature on the molar ratio of 2-butene to 1-butene produced from *n*-butane dehydrogenation, measured with 2.53 kPa *n*-butane/He and WHSV = 87 h⁻¹.

conversion decreased from 66.0 to 19.7%). Cofeeding hydrogen also leads to a decrease in 1,3-BD selectivity from around 37% to about 26%. Notably, the yield of 1,3-BD remains relatively stable at ca. 16–13% for 860 min of TOS, as seen in Figure S3B, in sharp contrast with the continuous decrease in 1,3-BD yield from 23.3 to 11.8% observed without cofed H₂.

3.2. Effect of Pt Content. Figure 2 shows the rates of *n*-butane dehydrogenation over 0.04Pt–0.36Zn–DeAlBEA for Pt/Al ratios of 0.04, 0.06, and 0.08 measured at 673 K and 2.53 kPa *n*-butane in He. These experiments were conducted with identical space-time relative to Pt. Under the conditions employed, the conversion of *n*-butane is less than 15% and the selectivity to dehydrogenation products is greater than 99.9%. As observed in Figure 2A, the rate of *n*-butane dehydrogenation normalized by catalyst mass increases linearly with the Pt content up to a Pt/Al ratio of 0.08. The rate of 1,3-BD formation normalized per gram of catalyst exhibits a trend similar to that for the rate of *n*-butane dehydrogenation, increasing linearly as the Pt/Al ratio increases. The rates of *n*-butane dehydrogenation and 1,3-BD formation normalized per Pt atom, the turnover frequency (TOF), are shown in Figure 2B. The TOFs for *n*-butane dehydrogenation and 1,3-BD formation are about 1.30 and 0.075 mol/mol Pt/s, respectively, and are nearly independent of the Pt content for Pt/Al ratios up to 0.08. These findings are consistent with the conclusion that the Pt sites in 0.04Pt–0.36Zn–DeAlBEA are predom-

inantly isolated.²⁴ The effect of the Pt/Al ratio on *n*-butane dehydrogenation was also measured at 573 K (see Figure S4) with the same findings, indicating that the apparent activation energy for *n*-butane dehydrogenation is independent of the Pt/Al ratio.

3.3. Effect of Reaction Temperature. Figure 3A,B shows the effects of reaction temperature on the conversion of *n*-butane, the overall dehydrogenation selectivity, as well as the initial product distribution for *n*-butane conversion on 0.04Pt–0.36Zn–DeAlBEA at TOS = 5 min. As the reaction temperature increases from 623 to 823 K, the conversion of *n*-butane increases monotonically from 13.1 to 66.0%, with a total dehydrogenation selectivity of >97.9%. Formation of C₁–C₃ products is barely observed at temperatures below 753 K and, as mentioned earlier, the highest selectivity to these products is 2.1% at 823 K (Figure 3B). Moreover, almost no deactivation is observed for *n*-butane conversion below 753 K (Figure 3A). This figure also shows that 1-butene and 2-butene are the dominant products at lower reaction temperatures (up to 753 K) and that the selectivity to 1,3-BD increases significantly with increasing temperature at the expense of *n*-butenes, consistent with the equilibrium product distribution with temperature shown in Figure S2A. More specifically, the selectivity to 1,3-BD over 0.04Pt–0.36Zn–DeAlBEA increases from 1.0 to 7.9% when the temperature increases from 623 to 723 K and then further increases to ca. 13.5 and 35.3% for 753 and 823 K, as seen in Figure 3B. The enhanced selectivity to

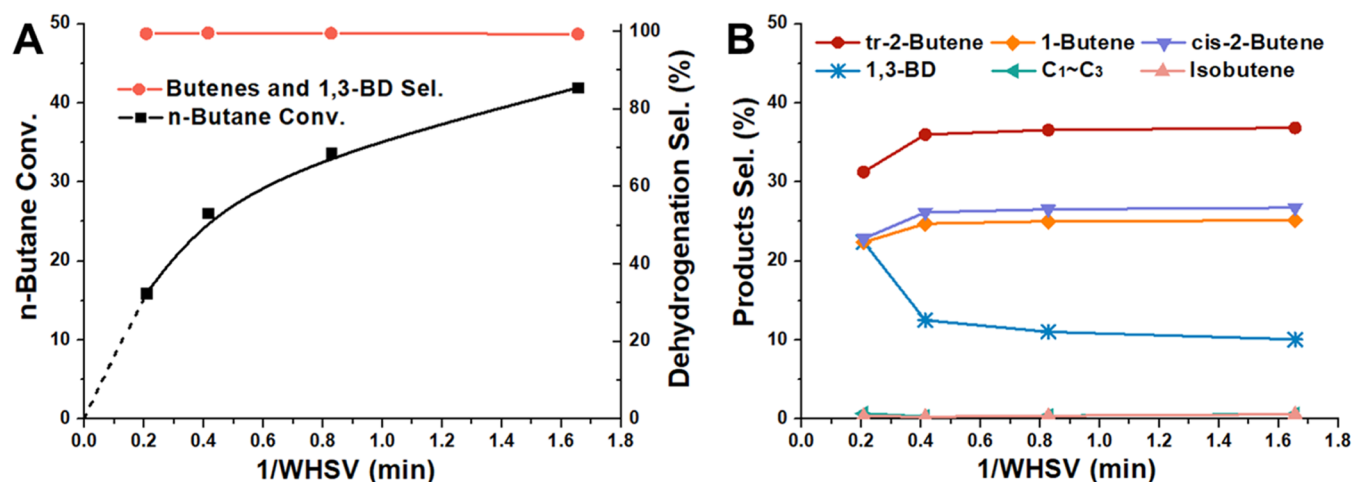


Figure 4. Effects of space-time on (A) the conversion of *n*-butane and overall selectivity to dehydrogenation products and (B) product distribution during *n*-butane conversion over 0.04Pt–0.36Zn-DeAlBEA measured at 753 K with 5.07 kPa *n*-butane/He. Reaction conditions: $m_{\text{cat}} = 10$ mg, total flow rates = 50–400 mL min⁻¹. The dashed line in panel (A) is a guide for the eye.

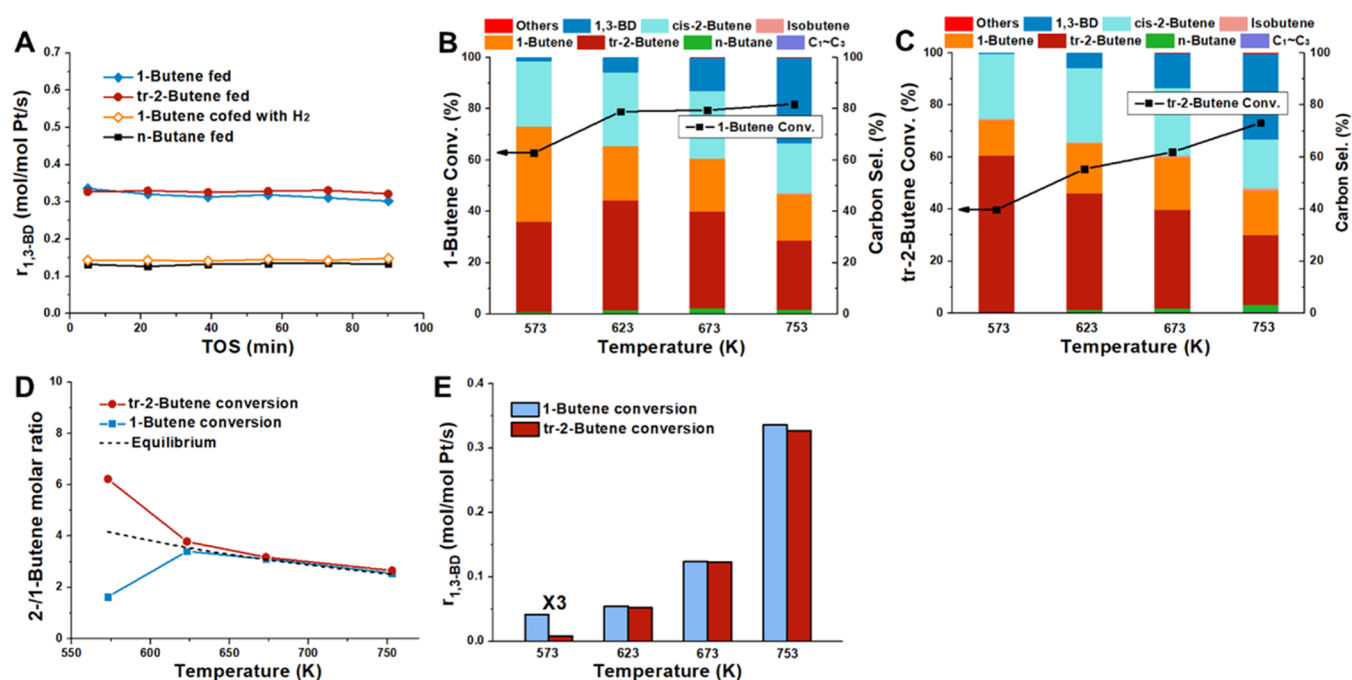


Figure 5. (A) Comparison of the rates of 1,3-BD formation from *n*-butane, 1-butene, *trans*-2-butene, and 1-butene/H₂ cofed with a molar ratio of 1:1 over 0.04Pt–0.36Zn-DeAlBEA at 753 K. (B) Conversion of 1-butene and product distribution observed over 0.04Pt–0.36Zn-DeAlBEA as a function of reaction temperature measured at TOS = 5 min. (C) Conversion of *trans*-2-butene and product distribution over 0.04Pt–0.36Zn-DeAlBEA as a function of reaction temperature measured at TOS = 5 min. (D) Molar ratio of 2-butene to 1-butene for 1-butene and *trans*-2-butene conversion on 0.04Pt–0.36Zn-DeAlBEA as a function of temperature. The dashed line shown in panel (D) is the 2-butene/1-butene molar ratios at equilibrium. (E) Rates of 1,3-BD formation from 1-butene and *trans*-2-butene conversion over 0.04Pt–0.36Zn-DeAlBEA as a function of temperature. The rates of 1,3-BD formation at 573 K are magnified 3X for the ease of observation. Reaction conditions: $m_{\text{cat}} = 10$ mg; dehydrogenation of butenes is conducted with 1.27 kPa 1-butene/He, 1.27 kPa *trans*-2-butene/He, and 1.27 kPa 1-butene/1.27 kPa H₂/He; conversion of *n*-butane is with 2.53 kPa *n*-butane/He; total flow rate = 80 mL min⁻¹.

1,3-BD with increasing temperature indicates that the activation energy for butene dehydrogenation to 1,3-BD is higher than that for *n*-butane dehydrogenation. Notably, the selectivity to 1,3-BD at thermal equilibrium increases from 1.2 to 8.6, 14.6, and 39.0% as the temperature increases from 623 to 723, 753, and 823 K for a feed containing 2.53 kPa of *n*-butane, respectively.

The molar ratios of *trans*-2-butene to *cis*-2-butene and 2-butene (including *trans*-2-butene and *cis*-2-butene) to 1-butene

produced from *n*-butane dehydrogenation with 2.53 kPa of *n*-butane at different temperatures were compared with the thermodynamically equilibrated product distribution (Figure S5). As shown, the molar ratios of both 2-/1-butene and *trans*-/*cis*-2-butene are close to those for equilibrium at each temperature and in agreement with the equilibrium distribution for *n*-butene isomerization reported previously.²⁷ Therefore, under the reaction conditions explored, the butene isomers formed by *n*-butane dehydrogenation rapidly establish

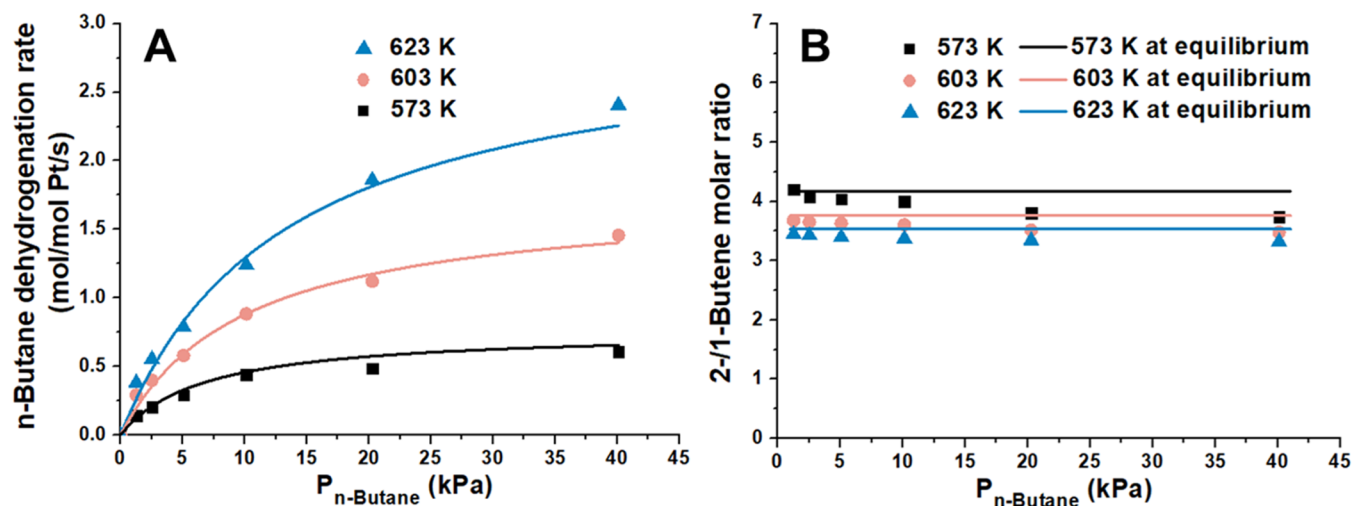


Figure 6. (A) Dependence of the rates of *n*-butane dehydrogenation and (B) the molar ratio of 2-butene/1-butene over 0.04Pt–0.36Zn-DeAlBEA measured at 573, 603, and 623 K on the *n*-butane partial pressure. Reaction conditions: $m_{\text{cat}} = 10$ mg, total flow rate = 240 mL min⁻¹. The lines shown in panel (A) are regressed fits of eq 1 to the data. The black line, pink line, and blue line in panel (B) show the molar ratios of 2-butene/1-butene at equilibrium and temperatures of 573, 603, and 623 K, respectively.

thermodynamic equilibrium even at 623 K. The only exception is isobutene, which is always found in concentration well below that expected for equilibrium. This suggests that skeletal isomerization of linear butenes is very slow over 0.04Pt–0.36Zn-DeAlBEA.

Rapid equilibration of butene isomers hinders the identification of the primary product (1-butene or 2-butene) formed during *n*-butane dehydrogenation. To that end, *n*-butane conversion over 0.04Pt–0.36Zn-DeAlBEA was measured at temperatures below 623 K and the space velocity was increased to 87 h⁻¹ for an *n*-butane feed partial pressure of 2.53 kPa. Under these differential conversion conditions, the formation of 1,3-BD and isobutene is negligible. As shown in Figure 3C, as the reaction temperature decreases, the molar ratio of 2-butene to 1-butene formed from *n*-butane dehydrogenation increases monotonically. It is also noted that the 2-butene/1-butene molar ratio falls increasingly below that for equilibrium as the temperature decreases to 523 K. This leads us to conclude that 1-butene is most likely formed as the primary product, which then undergoes rapid isomerization to 2-butene at higher temperatures and longer space-times. Therefore, even though 2-butene is the more stable product thermodynamically, the kinetics of 1-butene formation are preferred. We note that the experimental evidence does not allow us to exclude the possibility that some 2-butene is also formed directly by dehydrogenation of *n*-butane; however, this process appears to be slower than the formation of 1-butene.

3.4. Influence of Space-Time on the *n*-Butane Dehydrogenation. The effects of space-time, defined as the inverse of the weight-hourly space velocity (1/WHSV), on *n*-butane conversion and product selectivity over 0.04Pt–0.36Zn-DeAlBEA were investigated at 753 K. As seen in Figure 4A, with increasing space-time, the conversion of *n*-butane increases almost linearly for low space-times and then more slowly for higher space-times. At the same time, the overall selectivity to butenes and 1,3-BD shown in Figure 4B decreases slightly (from 99.8 to 99.3%) due to slightly increased *n*-butane cracking at higher space-time. Among the dehydrogenation products, the selectivity to *n*-butenes (*trans*-2-butene, *cis*-2-butene, and 1-butene) increases as the space-

time extends from 0.2 to 0.4 min and then almost reaches a plateau for 1/WHSV beyond 0.4 min. By contrast, there is an obvious decrease in the selectivity to 1,3-BD as the space-time increases from 0.2 to 0.4 min and then decreases further but at a very slow rate for longer space-times. A plausible explanation for the decreased 1,3-BD selectivity at higher space-time is the hydrogenation of 1,3-BD to butenes on 0.04Pt–0.36Zn-DeAlBEA.^{28–30} This interpretation is supported by the decrease in 1,3-BD selectivity when H₂ is cofed with either *n*-butane (Figure S3) or 1-butene (see Figure 5A). Even further evidence for the proposed hydrogenation process over 0.04Pt–0.36Zn-DeAlBEA is indicated by the molar ratio of ethane to ethylene, which is 2 in this case. If ethane and ethylene were solely formed via the central cracking of *n*-butane, a molar ratio of close to unity would be expected.

3.5. Dehydrogenation of 1-Butene and 2-Butene to 1,3-BD. We next explored the reactions of 1-butene and 2-butene catalyzed by 0.04Pt–0.36Zn-DeAlBEA to identify the precursor to 1,3-BD. These experiments were undertaken at reaction conditions comparable to those used for *n*-butane dehydrogenation. Figure 5A shows identical rates of 1,3-BD formation from 1-butene and *trans*-2-butene for the same reactant feed partial pressure, suggesting that 1-butene is rapidly equilibrated with 2-butene prior to the dehydrogenation of butene to 1,3-BD. Evidence for rapid isomerization of 1- and 2-butenes is also seen in Figure 5B,C (the rightmost columns). The carbon distributions for 1-butene and *trans*-2-butene conversion are nearly identical and have the same molar ratio of 2-butene to 1-butene (2.60) (Figure 5D), which is very close to that calculated for thermodynamic equilibrium at 753 K (2.51) given by the dashed line (Figure 5D).

Figure 5A also shows that the rates of 1,3-BD formation from 1-butene and *trans*-2-butene are 2.4 times higher than that produced from *n*-butane as the reactant. It should be noted that while the feed partial pressures of 1-butene and *trans*-2-butene were both 1.27 kPa, the partial pressure of *n*-butane was 2.57 kPa. For this partial pressure of *n*-butane at 753 K, Figure 3A shows that the conversion of *n*-butane is about 50% and the total selectivity to butenes and 1,3-BD is higher than 99.3%; however, the selectivity to isobutene for

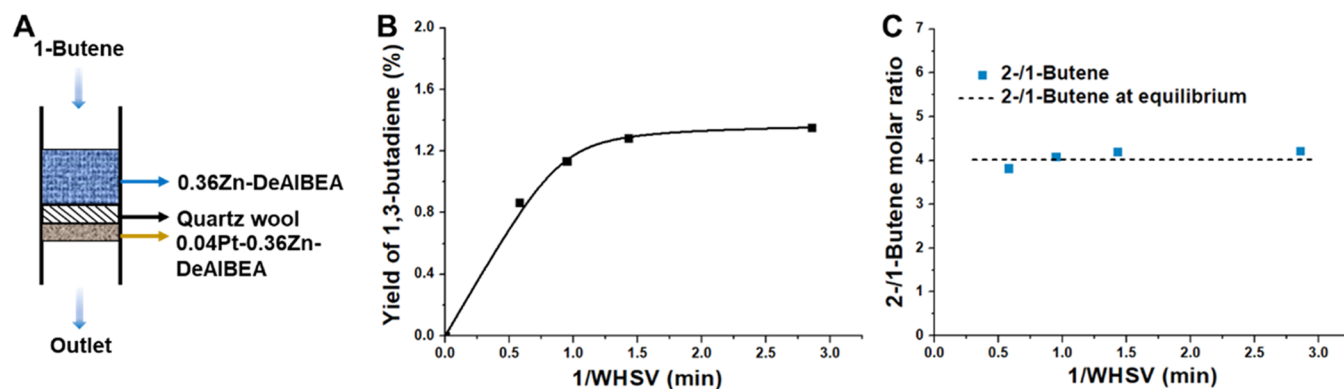


Figure 7. (A) Schematic illustration of the catalyst bed. 0.04Pt–0.36Zn–DeAlBEA is packed below 0.36Zn–DeAlBEA, separated by an inert layer of quartz wool. Effects of space-time on (B) the yield of 1,3-BD and (C) the molar ratios of 2-butene/1-butene for 1-butene reaction over 0.36Zn–DeAlBEA and 0.04Pt–0.36Zn–DeAlBEA at 583 K. Reaction conditions: $m_{\text{cat}} = 150$ mg of 0.36Zn–DeAlBEA and 5 mg 0.04Pt–0.36Zn–DeAlBEA, $P_{1\text{-Butene}} = 1.91$ kPa, total flow rates = 40–197 mL min^{-1} . Before 1-butene contacts 0.04Pt–0.36Zn–DeAlBEA, equilibrium for 1-butene isomerization is achieved for the space-time >0.63 min over the upper 0.36Zn–DeAlBEA catalyst layer.

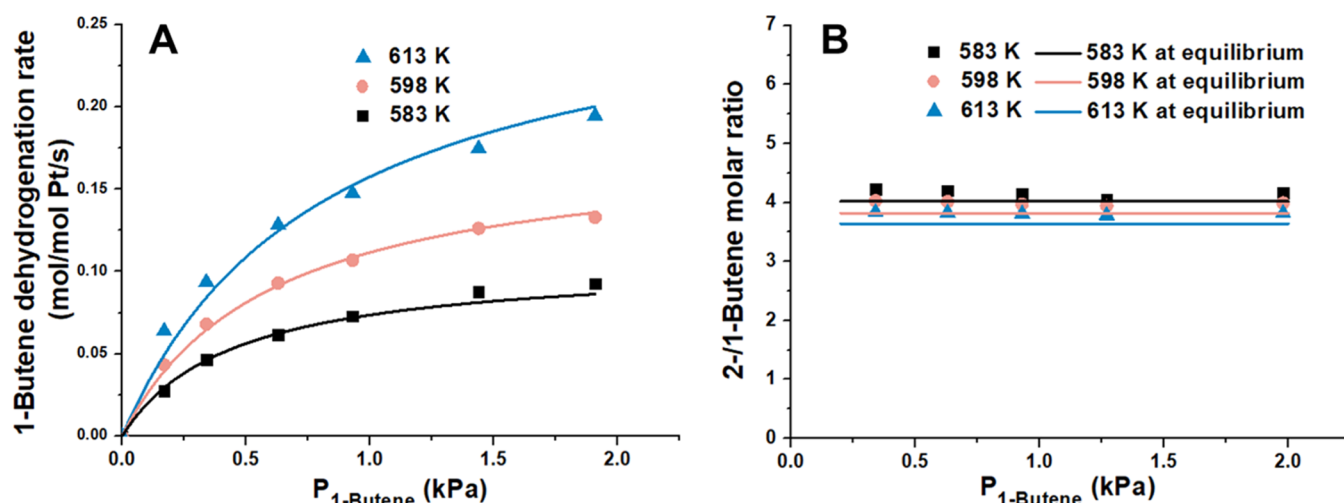


Figure 8. (A) Dependence of the rates of 1-butene dehydrogenation and (B) the molar ratio of 2-butene/1-butene over 0.04Pt–0.36Zn–DeAlBEA measured at 583, 598, and 613 K on the 1-butene partial pressure. Reaction conditions: $m_{\text{cat}} = 150$ mg of 0.36Zn–DeAlBEA and 5 mg of 0.04Pt–0.36Zn–DeAlBEA, total flow rates = 120 mL min^{-1} . The lines shown in panel (A) are regressed fits of eq 2 to the data. The lines shown in panel (B) are thermodynamic equilibrium molar ratios of 2-butene to 1-butene at each temperature.

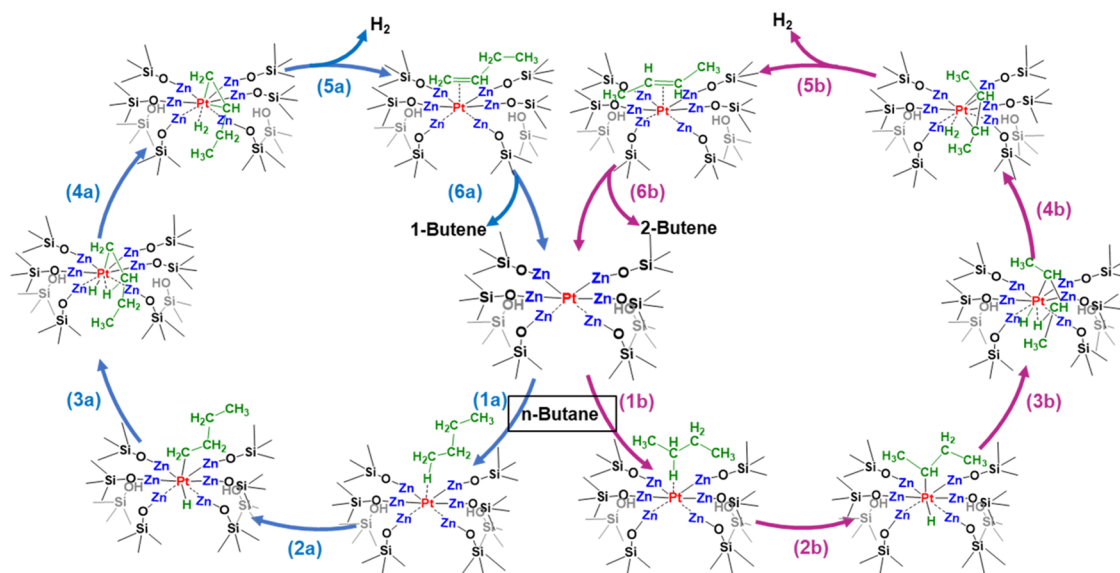
these conditions is only $\sim 0.8\%$. Consequently, the primary products of *n*-butane dehydrogenation are equimolar proportions of *n*-butenes and H_2 (ca. 1.27 kPa each). To identify how the presence of H_2 affects the formation of 1,3-BD, an equimolar mixture of 1-butene and H_2 (each at 1.27 kPa in a balance of He) was fed to the reactor. In this case, Figure 5A shows that the rate of 1,3-BD formation decreases from 0.34 mol/mol Pt/s in 1.27 kPa 1-butene to 0.143 mol/mol Pt/s, which is almost the same rate as that formed from *n*-butane (0.133 mol/mol Pt/s) (yellow and black lines in Figure 5A). As discussed below, the lower rate of 1,3-BD formation when 1-butene and H_2 are present is attributed to the partial hydrogenation of 1,3-BD to butenes.

Further exploration of 1-butene and *trans*-2-butene conversion at a lower reaction temperature, ranging from 673 to 573 K, was conducted to move the ratio of isomerization products away from equilibrium and thereby provide the possibility for distinguishing the precursor to 1,3-BD. Figure 5D clearly shows that the 2-butene/1-butene ratio gradually deviates from equilibrium as the temperature decreases. At 573 K, we observe that the rate of 1,3-BD formation from 1-butene

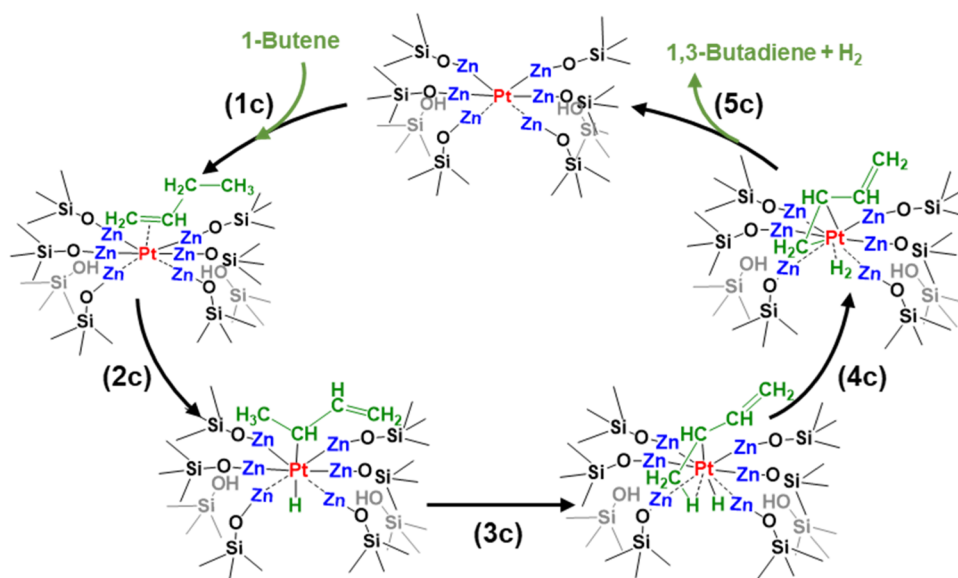
is 5 times higher than that from *trans*-2-butene for an identical reactant partial pressure (Figure 5E). Consequently, 1-butene is proposed to be the precursor to 1,3-BD rather than *trans*-2-butene.

3.6. Kinetics of *n*-Butane Dehydrogenation to Butene. Based upon the studies of space-time effects on *n*-butane dehydrogenation (Figure S6), kinetics for *n*-butane dehydrogenation were measured using a total flow rate of 240 mL min^{-1} ($1/\text{WHSV} < 0.75$ min) and temperatures below 623 K. Under these conditions, the dehydrogenation of *n*-butane is far from thermodynamic equilibrium and the selectivity to 1,3-BD and $\text{C}_1\text{--C}_3$ products is below 2 and 0.1%, respectively.

The dependence of the turnover frequency (per Pt atom) (TOF) for *n*-butane dehydrogenation on the *n*-butane partial pressure, measured under differential reaction conditions (conversion < 6.5%), is shown in Figure 6A. At all three temperatures (623, 603, and 573 K), the rate of *n*-butane dehydrogenation increases linearly with *n*-butane partial pressure at low *n*-butane partial pressures, after which it increases with less than a first-order dependence. Figure 6B shows the dependence of the molar ratio of 2-butene/1-butene

Scheme 1. Reaction Mechanism for the Dehydrogenation of *n*-Butane to *n*-Butenes over 0.04Pt–0.36Zn-DeAlBEA

Scheme 2. Reaction Mechanism for the Dehydrogenation of 1-Butene to 1,3-BD over 0.04Pt–0.36Zn-DeAlBEA



as a function of the *n*-butane partial pressure. At each temperature, the molar ratio of 2-butene/1-butene is nearly independent of the *n*-butane partial pressure and close to the equilibrium ratio. The slight decrease in 2-butene/1-butene ratio below the equilibrium value with increasing *n*-butane partial pressure observed for 573 K is ascribed to the decreasing *n*-butane space-time and low temperature.

3.7. Kinetics of 1-Butene Dehydrogenation to 1,3-BD.

The kinetics of 1-butene dehydrogenation to 1,3-BD, need to be carried out in such a way that *n*-butene isomerization is equilibrated and the hydrogenation of 1,3-BD is avoided. The first issue can be circumvented using a quasi-equilibrated mixture of 1-butene and 2-butene as the feed, and the second issue can be minimized by reducing the space-time to avoid secondary hydrogenation. (See the Supporting Information, Figure S10, for a discussion of this point.) We note that it is almost impossible to realize these two goals at the same time using only 0.04Pt–0.36Zn-DeAlBEA as the catalyst (Figure

S8). As presented in Figure S8C, long space-times are necessary to achieve the thermodynamic equilibrium of *n*-butene isomers. However, as indicated by the yield of 1,3-BD and *n*-butane in Figures S8B and S10, long space-times result in unwanted secondary hydrogenation of 1,3-BD to butenes and butenes to butane. To avoid this problem, a catalyst layer above the 0.04Pt–0.36Zn-DeAlBEA layer is needed to achieve quasi-equilibration of 1-butene and 2-butene isomers; however, this catalyst should have negligible butene dehydrogenation activity relative to 0.04Pt–0.36Zn-DeAlBEA. To achieve this objective, we used a dual-layer catalyst bed containing 150 mg of 0.36Zn-DeAlBEA placed above a layer of 5 mg of 0.04Pt–0.36Zn-DeAlBEA, separated with inert quartz wool (Figure 7A). With increasing space-time (based on 0.04Pt–0.36Zn-DeAlBEA), the yield of 1,3-BD increases almost linearly for 1/WHSV < 1 min and then increases more slowly with longer space-time (Figure 7B). Figure 7C

also shows that for all space-times, the ratio of 2-butene/1-butene remains at its equilibrium value.

Having established that 1-butene rapidly achieves isomerization equilibrium at 583 K and higher, measurements of the kinetics of 1-butene dehydrogenation to 1,3-BD were obtained between 583 and 613 K. The rate of 1,3-BD formation as functions of 1-butene partial pressure and temperature is shown in Figure 8A. At all three temperatures (583, 598, and 613 K), the rate of 1,3-BD formation exhibits a Langmuir–Hinshelwood dependence on 1-butene partial pressure. At low partial pressures, the rate of 1-butene dehydrogenation exhibits a first-order dependence on 1-butene partial pressure, while at high partial pressure, the order decreases to less than 1 and then approaches 0. In addition, the molar ratio of 2-butene to 1-butene exhibits a weak dependence on the reaction temperature, increasing as temperature increases, as seen in Figure 8B. Over the range of 1-butene partial pressure studied, the 2-butene/1-butene ratio is almost independent of 1-butene partial pressure and slightly higher than that for thermodynamic equilibrium due to further dehydrogenation of 1-butene to 1,3-BD.

3.8. Reaction Mechanism for *n*-Butane Dehydrogenation to 1,3-BD over 0.04Pt–0.36Zn–DeAlBEA. Schemes 1 and 2 illustrate possible reaction mechanisms for *n*-butane dehydrogenation to *n*-butenes and subsequent 1-butene dehydrogenation to 1,3-BD. The first step is the adsorption of *n*-butane, which proceeds by either the interaction of one methyl H with a Pt atom (step 1a) or the interaction of a methylene H with a Pt atom (step 1b). These two interactions are suggested by DFT studies of propane dehydrogenation over a Pt₃X (X = Ir, Sn, Ge, and Si) cluster model and *n*-butane adsorption on Ni–Sn-supported SiO₂.^{31,32} In the first case, *n*-butane adsorbed on Pt sites undergoes α -hydride abstraction of the adsorbed methyl group (step 2a), leading to an intermediate with the abstracted H atom and butyl fragment connected to the same Pt single site. The subsequent second hydrogen abstraction from an adjacent methylene group of the butyl fragment produces 1-butene and H₂ (steps 3a and 4a).¹⁷ Alternatively, *n*-butane interacts with a Pt atom through the methylene hydrogen and produces an intermediate with *sec*-butyl fragment and the abstracted H atom both attaching to the Pt atom (step 2b). After this step, the C–H bond at the methylene group cleaves and 2-butene and H₂ are formed. H₂ and 1-butene or 2-butene desorb from the active sites. We note that the first α -hydride abstraction from a terminal methyl group (step 2a) is projected to have a slightly lower barrier compared with the C–H bond cleavage at the methylene group (step 2b), as was found theoretically over Pt₄X clusters.³¹ Consequently, 1-butene formation is expected to be favored kinetically, which is consistent with our experimental results. For the mechanism of 1-butene dehydrogenation to 1,3-BD, we envision that a part of the 1-butene generated from *n*-butane dehydrogenation does not desorb from the active sites but undergoes further dehydrogenation to produce 1,3-BD and H₂. Specifically, as given in Scheme 2, a facile, heterolytic C–H cleavage in the methylene group of adsorbed 1-butene occurs first, followed by the rate-limiting α -hydride elimination to produce 1,3-BD and H₂. Finally, the desorption of 1,3-BD and H₂ completes the catalytic cycle.

Based upon the reaction sequences illustrated in Schemes 1 and 2, the rate expressions for *n*-butane and 1-butene dehydrogenation can be represented as eqs 1 and 2,

respectively. For both reactions, the rate-limiting step is assumed to be the dissociative adsorption of *n*-butane or 1-butene (steps 2a and 2b in Scheme 1 and step 2c in Scheme 2), based on the findings reported for propane and *n*-butane dehydrogenation over Pt-based catalysts.^{17,18,31} The adsorption of *n*-butane or butene is taken to be quasi-equilibrated, and the occupancy of Pt sites by all reaction intermediates is taken to be negligible. The concentrations of reaction products, butene, 1,3-BD, and *n*-butane are obtained by applying the pseudo-steady-state hypothesis. Derivation of eqs 1 and 2 is described in the Supporting Information. Based upon the observed kinetics, we propose

$$r_{C_4^-} = \frac{k_1 K_{C_4^-} P_{C_4^-}}{1 + K_{C_4^-} P_{C_4^-}} \quad (1)$$

$$r_{C_4^=} = \frac{k_2 A K_{C_4^=} P_{C_4^=}}{1 + K_{C_4^=} P_{C_4^=}} \quad (2)$$

In eqs 1 and 2, $r_{C_4^-}$ and $r_{C_4^=}$ are the turnover rates of *n*-butane and 1-butene dehydrogenation per Pt site, respectively; and $P_{C_4^-}$ and $P_{C_4^=}$ are the partial pressure of *n*-butane and 1-butene fed, respectively. The parameters $K_{C_4^-}$ and $K_{C_4^=}$ represent the equilibrium constants for the adsorption of *n*-butane and *n*-butenes on the Pt sites, respectively; k_1 and k_2 are the dehydrogenation rate constants of *n*-butane and 1-butene, respectively; and A represents the mole fraction of 1-butene in the total *n*-butenes at thermal equilibrium.

As discussed above, the kinetics of *n*-butane dehydrogenation were carried out for *n*-butane conversions <6.4% at the highest temperature and the lowest *n*-butane partial pressure and <5% for all other reaction conditions. Under these conditions, the concentration of butenes is insignificant compared with that of reactant *n*-butane and the secondary dehydrogenation of 1-butene to 1,3-BD is expected to be very low. Moreover, as evidenced by the space-time study of *n*-butane dehydrogenation, the conversion of *n*-butane exhibits a first-order dependence on space-time ($1/\text{WHSV} < 0.75$ min), suggesting that the hydrogenation of butene and other secondary reactions are negligible. Consequently, the inhibition by butenes and 1,3-BD can be eliminated. Accordingly, at a very low partial pressure of *n*-butane, the rate of *n*-butane dehydrogenation is first-order in *n*-butane partial pressure, but at higher *n*-butane partial pressure, the order in *n*-butane partial pressure decreases to less than 1. This trend is consistent with the experimental result shown in Figure 6A.

The kinetics of 1-butene dehydrogenation to 1,3-BD were measured so that 1,3-BD accounted for <8% of the total C₄ components, i.e., 1-butene, 2-butene, 1,3-BD, and *n*-butane. The influence of *n*-butane is not likely to be significant since the yield of *n*-butane is always lower than 0.15%. Moreover, Figure 7B shows that the yield of 1,3-BD is nearly first-order in space-time with $1/\text{WHSV} < 0.95$ min, suggesting that the hydrogenation of 1,3-BD and butenes is negligible. Similarly, the inhibition of the rate of 1-butene dehydrogenation due to 1,3-BD and *n*-butane is regarded as insignificant. In this case, the rate expression of 1-butene dehydrogenation (eq 2) exhibits a first-order dependence in 1-butene partial pressure at low partial pressures but then becomes less strongly dependent on the 1-butene partial pressure at higher values, in a manner similar to that observed experimentally (Figure 8A).

Equations 1 and 2 were fit to the measured rate data shown in Figures 6 and 7 via nonlinear least-squares regression. The quality of the fit was assessed by the parity plot shown in Figure S11. The value of R^2 with respect to the dehydrogenation rate of both *n*-butane and 1-butene reach up to 0.99, indicating good agreement between experimental and model estimated data.

The adsorption enthalpy of *n*-butane and the intrinsic activation energy for *n*-butane dehydrogenation were obtained from a van't Hoff plot of the equilibrium adsorption constant for *n*-butane and an Arrhenius plot of the rate constant (Figure S12). As shown in Table 1, the calculated enthalpy for *n*-

Table 1. Rate Parameters and Experimental Measured Adsorption Enthalpy of *n*-Butane as well as Intrinsic Activation Energy for *n*-Butane Dehydrogenation over 0.04Pt–0.36Zn–DeAlBEA

rate parameters		$K_{C_4^-}$, kPa ⁻¹	k_1 , mol mol Pt ⁻¹ s ⁻¹
T, K	623	0.075	3.0
	603	0.101	1.75
	573	0.149	0.77
entry	<i>n</i> -butane ΔH_{ads} , kJ/mol	–40.1	
	intrinsic E_a , kJ/mol		80.8

butane adsorption (ΔH_{ads}) is –40.1 kJ/mol. This value is lower (less negative) than that reported for a Pt(111) surface, for which the adsorption enthalpy for *n*-butane ranges from –46.3 to –59.8 kJ/mol.^{33,34} The experimentally measured intrinsic activation energy for *n*-butane dehydrogenation is 80.8 kJ/mol, which is lower than the values of 129.4 kJ/mol over Pt/Mg(Al)(In)O³⁵ and 117.2 kJ/mol over PtSn/Al₂O₃.^{36,36} Given the similarity of the reaction mechanisms for propane and *n*-butane dehydrogenation over 0.04Pt–0.36Zn–DeAlBEA, a comparison can be made between the enthalpies of propane and *n*-butane.²⁴ The enthalpy of adsorption for propane is reported to be –29.3 kJ/mol, which is 10.8 kJ/mol higher than that of *n*-butane adsorption on the same catalyst. The measured activation energy for *n*-butane dehydrogenation is 9.2 kJ/mol lower than that for propane dehydrogenation reported before, which corresponds to a 6-fold difference between the first-order rate coefficients for the two reactions at 623 K, assuming a common entropy of activation for the two alkanes. Consistent with this expectation, the rate coefficient of *n*-butane at 623 K is about 7.9 times higher than that projected for propane dehydrogenation over 0.04Pt–0.36Zn–DeAlBEA.

The fitted rate parameters for 1-butene dehydrogenation over 0.04Pt–0.36Zn–DeAlBEA are given in Table 2. The

Table 2. Rate Parameters and Experimental Measured Adsorption Enthalpy of 1-Butene as well as Intrinsic Activation Energy for 1-Butene Dehydrogenation over 0.04Pt–0.36Zn–DeAlBEA

rate parameters		$K_{C_4^-}$, kPa ⁻¹	k_2 , mol mol Pt ⁻¹ s ⁻¹	A
T, K	613	1.20	1.34	0.22
	598	1.66	0.87	0.21
	583	2.26	0.54	0.20
entry	1-butene ΔH_{ads} , kJ/mol	–62.2		
	intrinsic E_a , kJ/mol		90.3	

enthalpy of 1-butene adsorption is estimated as –62.2 kJ/mol, which is lower (more negative) than that for *n*-butane adsorption. For comparison, studies of 1-butene adsorption on the surface of Pt(111) and on a Sn–Pt alloy with varying Sn concentrations are reported to have an adsorption energy of –73.2 and –56.4 kJ/mol; thus, our fitted value lies within this range. The intrinsic activation energy, calculated for k_2 , is 90.3 kJ/mol, as estimated from Figure S13B, which is higher than that obtained for *n*-butane dehydrogenation (80.8 kJ/mol).

Comparison of the activity and selectivity of 0.04Pt–0.36Zn–DeAlBEA with previously reported Pt-based catalysts is very difficult since most of these studies were carried out with different feed compositions, space-times, and temperatures. Also, none of the previously reported studies reported the detailed kinetics of *n*-butane dehydrogenation to butene or butene dehydrogenation to 1,3-BD. Furthermore, the *n*-butane conversion in prior studies was moderate to high, and in many cases, it was close to the equilibrium value, making it very difficult to compare the intrinsic activity of one catalyst to another. To enable such a comparison, we developed an approach for estimating the effective forward rate constants for *n*-butane dehydrogenation to butene (k_{1f}) and butene dehydrogenation to 1,3-BD (k_{2f}) using eqs 3 and 4, respectively. In doing so, we assumed that *n*-butane dehydrogenation occurred in a plug-flow reactor, whereas the dehydrogenation of butene occurred in a continuously stirred tank reactor. The latter assumption was deemed appropriate since the conversion of butene to 1,3-BD was relatively low in all cases. The assumptions and full derivations of these equations are provided in the Supporting Information

$$k_{1f} = \frac{F_{C_4^-}^0}{m} \int_0^X \frac{1}{\left[\frac{P_{C_4^-}^0(1-X)}{1+y_{C_4^-}^0 X} - \frac{P_{C_4^-}^0 X(X+\theta_{H_2})}{K_1(1+y_{C_4^-}^0 X)^2} \right]} dX \quad (3)$$

$$k_{2f} = \frac{r_{1,3-BD}}{\left[\frac{P_{C_4^-}^0 X(1-\text{Sel}_{C_4^-})}{1+y_{C_4^-}^0 X} - \frac{P_{C_4^-}^0 X \text{Sel}_{C_4^-} (X + X \text{Sel}_{C_4^-} + \theta_{H_2})}{K_2(1+y_{C_4^-}^0 X)^2} \right]} \quad (4)$$

In eqs 3 and 4, k_{1f} and k_{2f} are the effective forward rate constants for *n*-butane dehydrogenation and butene dehydrogenation, respectively; $P_{C_4^-}^0$ and $F_{C_4^-}^0$ are the inlet partial pressure and molar flow rate of *n*-butane, respectively; X and $\text{Sel}_{C_4^-}$ are the overall conversion of *n*-butane and selectivity to 1,3-BD, respectively; $y_{C_4^-}^0$ is the inlet mole fraction of *n*-butane; θ_{H_2} is the inlet molar ratio of cofed H₂ to *n*-butane; K_1 is the equilibrium constant for *n*-butane dehydrogenation to butene and H₂; K_2 is the equilibrium constant for 1-butene dehydrogenation to 1,3-BD and H₂; m means the mass of Pt; and $r_{1,3-BD}$ is the formation rate of 1,3-BD.

Figure 9 compares the calculated values of k_{1f} and k_{2f} for 0.04Pt–0.36Zn–DeAlBEA with those for 10 other Pt-based catalysts reported in the literature that have been used for *n*-butane dehydrogenation to butene and, in some cases, the dehydrogenation of butene to 1,3-BD. The elemental composition of each catalyst is given in Table 3, and Table S2 summarizes the reaction conditions, catalytic activity for each catalyst, and values of k_{1f} and k_{2f} at the temperature used in each study. Effective first-order forward rate constants for 0.04Pt–0.36Zn–DeAlBEA at a temperature between 673 and 898 K were projected using the calculated values at 823 K

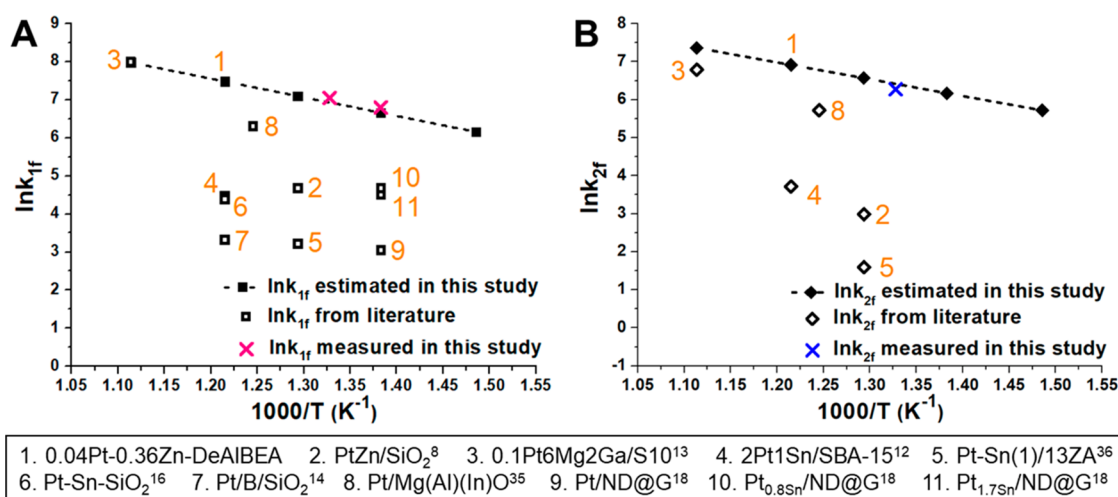


Figure 9. Comparison of the values of (A) k_{1f} and (B) k_{2f} for 0.04Pt–0.36Zn-DeAlBEA (catalyst 1) with values reported previously for Pt-based catalysts (catalysts 2–11, open symbols). Further details for each catalyst are given in Tables 3 and S2. The black dashed line in panel (A) is estimated based on the k_{1f} value at 823 K and the apparent activation energy of *n*-butane dehydrogenation for 0.04Pt–0.36Zn-DeAlBEA. The black dashed line in panel (B) is estimated based on the k_{2f} value at 823 K and the apparent activation energy of 1-butene dehydrogenation to 1,3-BD for 0.04Pt–0.36Zn-DeAlBEA. For verification, values of k_{1f} for experiments conducted at other temperatures over 0.04Pt–0.36Zn-DeAlBEA are calculated with eq 3 and presented as red crosses in panel (A). The blue cross in panel (B) is the value of k_{2f} for 1-butene dehydrogenation to 1,3-BD at 753 K calculated using eq E33 (Supporting Information).

Table 3. Elemental Composition of *n*-Butane Dehydrogenation Catalysts in Figure 9

no.	catalyst	metal loading, wt %			ref
		Pt	second metal	third metal	
1	0.04Pt–0.36Zn-DeAlBEA	0.73	2.36 (Zn)		this work
2	PtZn/SiO ₂	0.60	9.90 (Zn)		8
3	0.1Pt6Mg2Ga/S10	0.093	1.99 (Ga)	5.97 (Mg)	13
4	2Pt1Sn/SBA-15	3.00	0.91 (Sn)		12
5	Pt–Sn(1)/13ZA	2.00	1.20 (Sn)	13 (Zr)	37
6	Pt–Sn–SiO ₂	3.00	1.83 (Sn)		16
7	Pt/B/SiO ₂	0.021	0.595 (B)		14
8	Pt/Mg(Al)(In)O	0.89	0.171 (In)		35
9	Pt/ND@G	0.5			18
10	Pt _{0.8Sn} /ND@G	0.5	0.26 (Sn)		18
11	Pt _{1.7Sn} /ND@G	0.5	0.52 (Sn)		18

(using eqs 3 and 4) and the apparent activation energies for *n*-butane and 1-butene dehydrogenation determined from kinetics. The results are presented as solid black squares and diamonds in panels A and B, respectively. For further verification of the projected values of k_{1f} , values of this rate constant were also calculated at 723 and 753 K using eq 3 and are presented as red crosses in Figure 9A. In addition, the value of k_{2f} for 1-butene dehydrogenation to 1,3-BD at 753 K using 1-butene as the reactant was calculated assuming a plug-flow reactor and is shown as a blue cross in Figure 9B. Both sets of values are very close to the projected dashed lines, indicating that the apparent activation energies for k_{1f} and k_{2f} agree completely with those determined using the data in Tables 1 and 2. Figure S14 further compares the effective forward rate constants with the apparent first-order rate coefficients for *n*-butane dehydrogenation to butene ($k_1 K_{C_2^-}$) and 1-butene dehydrogenation to 1,3-BD ($k_2 AK_{C_2^-}$) determined from kinetic studies under differential conversions. As shown, the values of k_{1f} are only 10–35% lower than the apparent rate constant for temperature between 723 and 823 K, indicating good consistency between the rate constants determined from the

measured kinetic at low reactant conversion and values estimated from the effective forward rate constant. For the butene dehydrogenation to 1,3-BD, the values of k_{2f} are lower than those of $k_2 AK_{C_2^-}$. A possible explanation for this difference might be the exclusion of the effects of 1,3-BD adsorption, for which we do not know the adsorption constant.

The data in Figure 9 show that 0.04Pt–0.36Zn-DeAlBEA exhibits values of k_{1f} and k_{2f} that are much higher than those for most of the catalysts reported. The only exception is 0.1Pt6Mg2Ga/S10, for which the value of k_{1f} is close to that for 0.04Pt–0.36Zn-DeAlBEA projected to be 898 K. We note, however, that the value of k_{2f} for the dehydrogenation of 1-butene to 1,3-BD for 0.04Pt–0.36Zn-DeAlBEA is projected to be $1.59 \times 10^3 \text{ mol (g Pt}\cdot\text{h}\cdot\text{bar)}^{-1}$ at 898 K, which is about 1.8 times higher than that reported for 0.1Pt6Mg2Ga/S10.

4. CONCLUSIONS

A systematic study of *n*-butane dehydrogenation to 1,3-BD reaction was conducted over isolated Pt atoms anchored to the framework of dealuminated Beta zeolite via Zn atoms in the form of ($\equiv\text{Si-O-Zn}$)₄₋₆Pt complexes. The reaction of *n*-

butane produces 1-butene, 2-butene, and 1,3-BD as the primary products. At 823 K, an *n*-butane partial pressure of 2.53 kPa, and a space-time of 14.5 h⁻¹, 1,3-BD is produced with an apparent turnover frequency of 0.45 mol 1,3-BD (mol Pt)⁻¹ s⁻¹ and a selectivity to 1,3-BD of 35.3%. Investigation of the reaction pathway indicates that *n*-butane first undergoes dehydrogenation to produce 1-butene, which then rapidly isomerizes to produce an equilibrated mixture of 1-butene and 2-butene. 1-Butene is the precursor for 1,3-BD formation. Both *n*-butane dehydrogenation to butene and 1-butene dehydrogenation to 1,3-BD reactions exhibit a Langmuir–Hinshelwood dependence on *n*-butane and 1-butene partial pressures, respectively; the rate is first-order in *n*-butane and 1-butene at low reactant partial pressures and then decreases to less than first-order at higher reactant partial pressures. Rate expressions for the kinetics of *n*-butane and 1-butene dehydrogenation, based on the proposed reaction mechanisms for both reactions, are in good agreement with experimental observations. The measured intrinsic activation energy for 1,3-BD formation from 1-butene is 90.3 kJ/mol, while that for the first *n*-butane dehydrogenation step is 80.8 kJ/mol. The isolated Pt sites in the form of (≡Si–O–Zn)_{4–6}Pt complexes exhibit the highest effective forward rate constant for butene dehydrogenation to 1,3-BD (*k*_{2f}) and among the best for *n*-butane dehydrogenation to butene (*k*_{1f}) relative to other Pt-based catalysts reported.

■ ASSOCIATED CONTENT

SI Supporting Information

The Supporting Information is available free of charge at <https://pubs.acs.org/doi/10.1021/acscatal.2c00059>.

Standard enthalpies of formation of *n*-butane and dehydrogenation products at 298.15 K and 1 bar obtained from NIST Webbook and PURE37 utilized in Aspen Plus (Table S1); supplemental reaction results (Figures S1 and S3–S10); evolution of the equilibrium conversion of *n*-butane and product distribution with temperature measured with 2.53 kPa *n*-butane/He and 1 bar (Figure S2); derivation of rate expressions and parity plots of the dehydrogenation rate of *n*-butane and 1-butene (Figure S11); Arrhenius plots and van't Hoff plots for *n*-butane and 1-butene dehydrogenation (Figures S12 and S13); derivation of the expressions of effective forward rate constants for *n*-butane dehydrogenation to butenes and *n*-butene dehydrogenation to 1,3-BD; summary of catalytic data for *n*-butane dehydrogenation catalysts reported previously (Table S2); and comparison of the effective forward rate constants with measured apparent rate constants over 0.04Pt–0.36Zn–DeAlBEA (PDF)

■ AUTHOR INFORMATION

Corresponding Author

Alexis T. Bell – Chemical Sciences Division, Lawrence Berkeley National Laboratory, Berkeley, California 94720, United States; Department of Chemical and Biomolecular Engineering, University of California, Berkeley, Berkeley, California 94720, United States; orcid.org/0000-0002-5738-4645; Email: alexibell@berkeley.edu

Authors

Yanfei Zhang – Chemical Sciences Division, Lawrence Berkeley National Laboratory, Berkeley, California 94720, United

States; Department of Chemical and Biomolecular Engineering, University of California, Berkeley, Berkeley, California 94720, United States

Liang Qi – Chemical Sciences Division, Lawrence Berkeley National Laboratory, Berkeley, California 94720, United States; Department of Chemical and Biomolecular Engineering, University of California, Berkeley, Berkeley, California 94720, United States

Branden Leonhardt – Chemical Sciences Division, Lawrence Berkeley National Laboratory, Berkeley, California 94720, United States; Department of Chemical and Biomolecular Engineering, University of California, Berkeley, Berkeley, California 94720, United States

Complete contact information is available at: <https://pubs.acs.org/10.1021/acscatal.2c00059>

Author Contributions

[§]Y.Z. and L.Q. contributed equally.

Notes

The authors declare no competing financial interest.

■ ACKNOWLEDGMENTS

This work was supported by the Office of Science, Office of Basic Energy Sciences (BES), of the U.S. Department of Energy (DOE) under Contract No. DE-AC02-05CH11231. L.Q. also acknowledges support from the Dalian Institute of Chemical Physics, Chinese Academy of Sciences, People's Republic of China.

■ REFERENCES

- (1) Makshina, E. V.; Dusselier, M.; Janssens, W.; Degreve, J.; Jacobs, P. A.; Sels, B. F. Review of old chemistry and new catalytic advances in the on-purpose synthesis of butadiene. *Chem. Soc. Rev.* **2014**, *43*, 7917–7953.
- (2) <https://www.databridgemarketresearch.com/reports/global-1-3-butadiene-market/> (accessed January 31, 2022).
- (3) White, W. C. Butadiene production process overview. *Chem.–Biol. Interact.* **2007**, *166*, 10–14.
- (4) Sushkevich, V. L.; Ivanova, I. I. Mechanistic study of ethanol conversion into butadiene over silver promoted zirconia catalysts. *Appl. Catal., B* **2017**, *215*, 36–49.
- (5) Sattler, J. J.; Ruiz-Martinez, J.; Santillan-Jimenez, E.; Weckhuysen, B. M. Catalytic dehydrogenation of light alkanes on metals and metal oxides. *Chem. Rev.* **2014**, *114*, 10613–10653.
- (6) Coperet, C. C–H bond activation and organometallic intermediates on isolated metal centers on oxide surfaces. *Chem. Rev.* **2010**, *110*, 656–680.
- (7) Kurokawa, H. Dehydrogenation of *n*-butane to butenes and 1,3-butadiene over PtAg/Al₂O₃ catalysts in the presence of H₂. *J. Mater. Sci. Chem. Eng.* **2018**, *6*, 16–24.
- (8) Camacho-Bunquin, J.; Ferrandon, M. S.; Sohn, H.; Kropf, A. J.; Yang, C.; Wen, J.; Hackler, R. A.; Liu, C.; Celik, G.; Marshall, C. L.; et al. Atomically precise strategy to a PtZn alloy nanocluster catalyst for the deep dehydrogenation of *n*-butane to 1, 3-butadiene. *ACS Catal.* **2018**, *8*, 10058–10063.
- (9) Nawaz, Z.; Fei, W. Pt–Sn-based SAPO-34 supported novel catalyst for *n*-butane dehydrogenation. *Ind. Eng. Chem. Res.* **2009**, *48*, 7442–7447.
- (10) Zhang, J.; Liu, X.; Blume, R.; Zhang, A. H.; Schlogl, R.; Su, D. S. Surface-modified carbon nanotubes catalyze oxidative dehydrogenation of *n*-butane. *Science* **2008**, *322*, 73–77.
- (11) Grub, J.; Löser, E. Butadiene. In *Ullmann's Encyclopedia of Industrial Chemistry*; Wiley, 2000.
- (12) Deng, L.; Miura, H.; Ohkubo, T.; Shishido, T.; Wang, Z.; Hosokawa, S.; Teramura, K.; Tanaka, T. The importance of direct

reduction in the synthesis of highly active Pt–Sn/SBA-15 for n-butane dehydrogenation. *Catal. Sci. Technol.* **2019**, *9*, 947–956.

(13) Chu, M.; Liu, Y.; Gong, J.; Zhang, C.; Wang, X.; Zhong, Q.; Wu, L.; Xu, Y. Suppressing dehydroisomerization boosts n-butane dehydrogenation with high butadiene selectivity. *Chem. – Eur. J.* **2021**, *27*, 11643–11648.

(14) Byron, C.; Bai, S.; Celik, G.; Ferrandon, M. S.; Liu, C.; Ni, C.; Mehdad, A.; Delferro, M.; Lobo, R. F.; Teplyakov, A. V. Role of boron in enhancing the catalytic performance of supported platinum catalysts for the nonoxidative dehydrogenation of n-butane. *ACS Catal.* **2020**, *10*, 1500–1510.

(15) Sun, Q.; Wang, N.; Fan, Q.; Zeng, L.; Mayoral, A.; Miao, S.; Yang, R.; Jiang, Z.; Zhou, W.; Zhang, J.; et al. Subnanometer bimetallic platinum–zinc clusters in zeolites for propane dehydrogenation. *Angew. Chem.* **2020**, *132*, 19618–19627.

(16) Deng, L.; Miura, H.; Shishido, T.; Wang, Z.; Hosokawa, S.; Teramura, K.; Tanaka, T. Elucidating strong metal-support interactions in Pt–Sn/SiO₂ catalyst and its consequences for dehydrogenation of lower alkanes. *J. Catal.* **2018**, *365*, 277–291.

(17) Zhang, J.; Deng, Y.; Cai, X.; Chen, Y.; Peng, M.; Jia, Z.; Jiang, Z.; Ren, P.; Yao, S.; Xie, J.; et al. Tin-assisted fully exposed platinum clusters stabilized on defect-rich graphene for dehydrogenation reaction. *ACS Catal.* **2019**, *9*, 5998–6005.

(18) Chen, X.; Peng, M.; Cai, X.; Chen, Y.; Jia, Z.; Deng, Y.; Mei, B.; Jiang, Z.; Xiao, D.; Wen, X. Regulating coordination number in atomically dispersed Pt species on defect-rich graphene for n-butane dehydrogenation reaction. *Nat. Commun.* **2021**, *12*, No. 7334.

(19) Chen, S.; Zhao, Z.-J.; Mu, R.; Chang, X.; Luo, J.; Purdy, S. C.; Kropf, A. J.; Sun, G.; Pei, C.; Miller, J. T.; et al. Propane dehydrogenation on single-site [PtZn₄] intermetallic catalysts. *Chem* **2021**, *7*, 387–405.

(20) Han, Z.; Li, S.; Jiang, F.; Wang, T.; Ma, X.; Gong, J. Propane dehydrogenation over Pt–Cu bimetallic catalysts: the nature of coke deposition and the role of copper. *Nanoscale* **2014**, *6*, 10000–10008.

(21) Cai, W.; Mu, R.; Zha, S.; Sun, G.; Chen, S.; Zhao, Z.-J.; Li, H.; Tian, H.; Tang, Y.; Tao, F. F.; et al. Subsurface catalysis-mediated selectivity of dehydrogenation reaction. *Sci. Adv.* **2018**, *4*, No. eaar5418.

(22) Liu, L.; Lopez-Haro, M.; Lopes, C. W.; Rojas-Buzo, S.; Concepcion, P.; Manzorro, R.; Simonelli, L.; Sattler, A.; Serna, P.; Calvino, J. J.; Corma, A. Structural modulation and direct measurement of subnanometric bimetallic PtSn clusters confined in zeolites. *Nat. Catal.* **2020**, *3*, 628–638.

(23) Cybulskis, V. J.; Bukowski, B. C.; Tseng, H. T.; Gallagher, J. R.; Wu, Z. W.; Wegener, E.; Kropf, A. J.; Ravel, B.; Ribeiro, F. H.; Greeley, J.; Miller, J. T. Zinc promotion of platinum for catalytic light alkane dehydrogenation: Insights into geometric and electronic effects. *ACS Catal.* **2017**, *7*, 4173–4181.

(24) Qi, L.; Babucci, M.; Zhang, Y.; Lund, A.; Liu, L.; Li, J.; Chen, Y.; Hoffman, A. S.; Bare, S. R.; Han, Y.; Gates, B. C.; Bell, A. T. Propane dehydrogenation catalyzed by isolated Pt atoms in ≡ SiOZn–OH nests in dealuminated zeolite Beta. *J. Am. Chem. Soc.* **2021**, *143*, 21364–21378.

(25) <https://www.aspentech.com/en/products/engineering/aspentech-plus/> (accessed January 31, 2022).

(26) <https://webbook.nist.gov/> (accessed January 31, 2022).

(27) Voge, H.; May, N. Isomerization equilibria among the n-butenes. *J. Am. Chem. Soc.* **1946**, *68*, 550–553.

(28) Sarkany, A.; Stefler, G.; Hightower, J. Participation of support sites in hydrogenation of 1, 3-butadiene over Pt/Al₂O₃ catalysts. *Appl. Catal., A* **1995**, *127*, 77–92.

(29) Lonergan, W. W.; Xing, X.; Zheng, R.; Qi, S.; Huang, B.; Chen, J. G. Low-temperature 1, 3-butadiene hydrogenation over supported Pt/3d/γ-Al₂O₃ bimetallic catalysts. *Catal. Today* **2011**, *160*, 61–69.

(30) Bertolini, J.-C. Surface stress and chemical reactivity of Pt and Pd overlayers. *Appl. Catal., A* **2000**, *191*, 15–21.

(31) Hauser, A. W.; Horn, P. R.; Head-Gordon, M.; Bell, A. T. A systematic study on Pt based, subnanometer-sized alloy cluster

catalysts for alkane dehydrogenation: effects of intermetallic interaction. *Phys. Chem. Chem. Phys.* **2016**, *18*, 10906–10917.

(32) Zhu, Q.; Wang, G.; Zhang, H.; Zhu, X.; Li, C. n-Butane dehydrogenation over Ni–Sn/SiO₂: Adsorption modes and reaction paths of n-butane and 1-butene. *Appl. Catal., A* **2018**, *566*, 113–120.

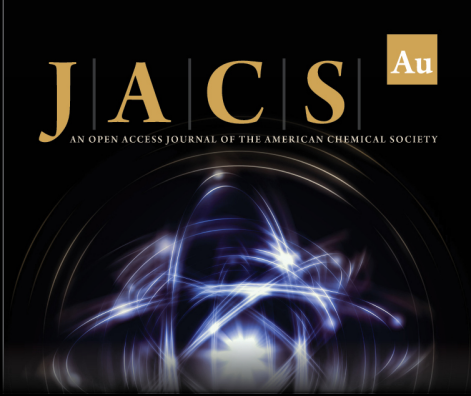
(33) Lee, K.; Morikawa, Y.; Langreth, D. C. Adsorption of n-butane on Cu (100), Cu (111), Au (111), and Pt (111): Van der Waals density-functional study. *Phys. Rev. B* **2010**, *82*, No. 155461.

(34) Lei, R. Z.; Gellman, A. J.; Koel, B. Desorption energies of linear and cyclic alkanes on surfaces: anomalous scaling with length. *Surf. Sci.* **2004**, *554*, 125–140.

(35) Wu, J.; Peng, Z.; Sun, P.; Bell, A. T. n-Butane dehydrogenation over Pt/Mg (In)(Al)O. *Appl. Catal., A* **2014**, *470*, 208–214.


(36) Natarajan, P.; Khan, H. A.; Yoon, S.; Jung, K.-D. One-pot synthesis of Pt–Sn bimetallic mesoporous alumina catalysts with worm-like pore structure for n-butane dehydrogenation. *J. Ind. Eng. Chem.* **2018**, *63*, 380–390.


(37) Larese, C.; Campos-Martin, J.; Fierro, J. Alumina-and zirconia–alumina-loaded tin–platinum. Surface features and performance for butane dehydrogenation. *Langmuir* **2000**, *16*, 10294–10300.



JACS Au
AN OPEN ACCESS JOURNAL OF THE AMERICAN CHEMICAL SOCIETY

Editor-in-Chief
Prof. Christopher W. Jones
Georgia Institute of Technology, USA

Open for Submissions 

pubs.acs.org/jacsau  ACS Publications
Most Trusted. Most Cited. Most Read.